JOINT EUROPEAN TORUS JET

JET–P(90)67

B.J.D. Tubbing, B. Balet, D.V. Bartlett, C.D. Challis, S. Corti, R.D. Gill,
C. Gormezano, C. Gowers, M. von Hellermann, M. Hugon, J.J. Jacquinot,
H. Jaeckel, P. Kupschus, K. Lawson, H. Morsi, J. O'Rourke,
D. Pasini, F. Rimini, G. Sadler, G.L. Schmidt
A. Tanga, F. Tibone. and JET Team

H-Mode Confinement in JET with Enhanced Performance by Pellet-Peaked Density Profiles

H-Mode Confinement in JET with Enhanced Performance by Pellet-Peaked Density Profiles

B.J.D. Tubbing, B. Balet, D.V. Bartlett, C.D. Challis, S. Corti, R.D. Gill, C. Gormezano, C. Gowers, M. von Hellermann, M. Hugon, J.J. Jacquinot, H. Jaeckel, P. Kupschus, K. Lawson, H. Morsi, J. O'Rourke, D. Pasini, F. Rimini, G. Sadler, G.L. Schmidt[1] A. Tanga, F. Tibone. and JET Team*

JET-Joint Undertaking, Culham Science Centre, OX14 3DB, Abingdon, UK

Princeton Plasma Physics Laboratory, New Jersey, USA
** See Appendix 1*

Preprint of Paper to be submitted for publication in
Nuclear Fusion

ABSTRACT.

The combination of two regimes of enhanced performance, the H mode and the pellet-enhanced-performance (PEP) mode, has been achieved in JET. The strong enhancement of the central plasma parameters, obtained with pellet injection and subsequent auxiliary heating, are found to persist well into the H mode phase. A characteristic of the PEP regime is that an improvement of the fusion reactivity over non-pellet discharges is obtained under the condition of near-equal electron and ion temperature. A maximum neutron production rate of $0.95 \cdot 10^{16}$ s^{-1} was obtained in a double-null X-point discharge with 2.5MW of neutral beam heating and 9MW of ion cyclotron resonance heating, with central ion and electron temperatures of about of 10keV and a central deuterium density of $8.0 \cdot 10^{19}$ m^{-3}. The corresponding fusion product $n_D T_i \tau_E$ is between 7.0 and $8.6 \cdot 10^{20}$ m^{-3}s keV. The enhanced neutron production is· predominantly of thermonuclear (maxwellian) origin. The compatibility of these regimes is an important issue in the context of tokamak ignition strategies. Several technical developments on JET have played a role in the achievement of this result: first, the use of low voltage plasma breakdown (0.15V/m) in order to permit pellet injection in an X-point configuration prior to formation of a q=1 surface; second, the elimination of ICRH specific impurities with antenna Faraday screens made of solid beryllium; third, the use of a novel system of plasma radial position control that stabilises the coupling resistance of the ion cyclotron heating system.

1 INTRODUCTION

The exploration of regimes of enhanced energy confinement in tokamaks is motivated by the observation that confinement is a critical issue for the design of next step devices, in which thermonuclear burn is the primary objective. The energy confinement, with its well—established dependence on plasma current, forces these devices to operate at rather high plasma current (12 to 30MA). This requirement has implications both for the size of the device and for the value of the toroidal field, both of which are important cost factors.

The basic regime of energy confinement in auxiliary heated tokamaks is the L (low) mode. Most of the proposed next step devices are not expected to reach ignition (NET [1], CIT [2], Ignitor [3], ITER [4]) under extrapolations of scaling laws for L mode energy confinement obtained on the present tokamaks, eg. [5,6,7]. Under somewhat more favourable extrapolations of data obtained mainly from JET [8], ignition in the L mode would be possible for a device operating with a plasma current of about 30MA [9]. Most of the proposed tokamaks thus rely on the further development of regimes of enhanced confinement, which have been established on various existing machines.

The primary regime of enhanced confinement is the H (high) mode, discovered in Asdex [10], and reproduced in many machines (PDX [11], JFT2—M [12], JET [13], DIII—D [14, JT60 [15], TFTR [16]). H mode confinement has been obtained with all the major auxiliary heating methods. In H mode, an increase in the energy confinement by a factor of two to three, compared to L mode, can be obtained. Although the physics of the enhancement are not yet understood, there is a general consensus that the primary element is the formation of a transport barrier at the plasma edge [17,18,19], resulting in high local pressure gradients. Modifications of the transport parameters in the bulk plasma are observed, which are believed to be the result of profile changes after the formation of the barrier [20].

A second regime of enhanced performance, using deep pellet injection and central ion cyclotron resonance heating (ICRH), has been proposed [21,22,23]. This pellet—enhanced—performance (PEP) mode was established first in JET L mode limiter discharges [24]. Similar results, but with neutral beam injection (NBI), were obtained in DIII [25], JT60 [26] and JFT2—M [27]. The PEP mode is obtained with strongly peaked density profiles, created by central ablation of a fuel pellet. In the PEP mode the core transport is reduced and the central plasma parameters, in particular the fusion reactivity, are strongly increased. There is a modest increase in global energy confinement.

It has been widely speculated, that the edge—related enhancement obtained in the H mode could be combined with the enhancement of the central parameters obtained in the PEP mode. In JFT2—M, a

transient improvement of the global energy confinement was obtained by injecting a pellet prior to the H mode transition, in discharges with NBI heating [27]. Initial results from JET, with moderate peaking of the density profile and with NBI heating, were reported [28]. In the remainder of this paper, we shall demonstrate that the combination of PEP mode and H mode has now been obtained, with strong density profile peaking, and with ICRH heating.

PEP modes are a transient phenomenon. In JET, the typical duration of the phase of enhanced reactivity is of order one second, which is about two energy confinement times. The termination of the enhanced phase is associated with the decay of the peaked density profile. Maintaining the peaked profile by further pellet injection during the enhanced phase is difficult because the high plasma temperature during the PEP mode prevents deep penetration of the pellet. Therefore, the applicability of the PEP mode as a mode of operation in long pulse ignited devices is limited, barring fundamental developments. However, for several of the proposed next step devices (CIT, Ignitor), the objective is to obtain a short ignited phase, with the aim of studying α particle physics. Ignition in these devices could be obtained at lower plasma currents or with lower auxiliary heating powers with the use of a PEP mode. Also, a transient increase of the α particle heating power could be a useful item in the ignition strategy in next step tokamaks. The following burn phase could then take place in a non pellet–enhanced H mode or L mode. Furthermore, the projected peak thermonuclear performance of JET in a deuterium–tritium plasma is considerably higher in the PEP mode than in the non–enhanced modes. For these reasons, a strong interest remains in this enhanced confinement regime, even when it is transient. We note that with the PEP mode, a high thermonuclear performance is obtained with ion and electron temperature approximately equal. This is in contrast to the high performance obtained in the hot–ion regime (supershots [29], hot–ion L mode [30], hot–ion H mode [31,32]) where the ion temperature significantly exceeds the electron temperature, and which can only be obtained with strong ion heating at low target densities.

2 DISCHARGES IN THE PEP–H MODE REGIME

The experiments were performed in a double–null magnetic separatrix configuration. The dominant power load is on the top X–point (this is accomplished by applying a 10 to 30mm upward vertical displacement to the plasma), which has the grad–B drift of ions directed towards the target area . The top X–point target area consists of 32 poloidal bands of carbon tiles. The distance from the X–point to the target tiles is about 20mm.

Evaporation of beryllium is applied during the night prior to the experiments. The evaporated layer on the X–point target area erodes off during the first plasma discharge after the evaporation. The beryllium coverage of the vessel walls results in a low concentration of the oxygen impurity through the gettering action of beryllium [33].

The ICRH system [34] has a total of eight antennas, situated in the horizontal mid–plane of the machine. The antennas are equipped with Faraday screens made of solid beryllium bars (see also next section), surrounded by carbon protection tiles which protrude about 20mm with respect to the screen. The antennas launch the fast ion cyclotron wave, and are used in a minority heating scheme with a hydrogen minority species in a deuterium plasma. The antennas are, for these experiments, operated in the toroidal dipole mode, where the currents in two adjacent conductors are in anti–phase.

The hydrogen minority, in the discharges presented here, was provided by gas puffing, prior to or during the heating period. Based on measurements with the neutral particle analyser, the ratio of hydrogen to deuterium is between 0.1 and 0.15, but there is considerable uncertainty as to the value within the plasma core, after the injection of the deuterium pellet.

Experiments were performed at toroidal fields of 2.8T (with an ICRH frequency of 43MHz) and 3.2T (with ICRH at 48MHz). Plasma currents were between 3 and 3.6MA.

In figure 1 the time evolution of the relevant parameters for a typical PEP–H mode discharge are shown. The toroidal field is 2.8T. The plasma current is 3MA, and reaches the flat top value at 4s. The formation of the X–point equilibrium, through the application of the shaping currents, is carried out at the end of the current rise. The objective of the early X–point formation (X–point formation in JET is normally done later, in the current flat top of the discharge; see also next section) is to avoid sawteeth prior to the pellet injection and PEP phases. The increase at about 4s of the vertical D_α signal, which has a line of sight near, but not at, the X–point target region, shows the X–point formation. The further increase of the D_α signal between 4.2 and 5.0s is due to gas–puffing, with the density control feedback system trying to maintain a constant density after the X–point formation. At 5.0s a deuterium pellet (4mm diameter, 4mm length, containing about $3\ 10^{21}$ D atoms) is injected with a speed of 1200m/s. The

injection is visible in the traces of the radiated power, the vertical D_α, the density and the temperature. The peaking of the density profile, characterised by the ratio of central to volume average density, is about 2.9 just after injection. The density profile just after injection is shown in figure 2a, as measured by the LIDAR time–of–flight Thomson scattering system [35]. Immediately after the injection the auxiliary heating is switched on. The NBI, at a level of 2.5MW (deuterium injection, with an energy of 80keV per particle) is required for the charge exchange recombination spectroscopy measurement of the ion temperature. The ICRH power is ramped up to 9MW in 0.5s.

The discharge is in PEP–L mode until 5.6s. During the PEP–L phase, the electron and ion temperatures, the plasma kinetic energy (measured by the diamagnetic loop), and the neutron production rate increase, while at the same time the volume average density and the central density decrease. At about 5.6s the transition to H mode takes place. The transition can be observed as an increase in the energy confinement time, a slight decrease of the vertical D_α signal (in other discharges, clearer D_α signatures have been obtained; an example is shown in figure 3) and a slight temporary decrease of the radiated power. At 5.75s, a single edge localised mode (ELM [10]) occurs. The stored energy increases to a level better than typical of H mode energy confinement: a maximum energy of 8.3MJ is reached at 6.2s. Profiles of the electron density and the electron temperature, as measured by the LIDAR system, are shown in figure 2a and 2b. Both the density and the temperature profiles show the large Shafranov shift; the profiles have their maximum at 3.4m, while the centre of the outer flux surface is at 3.1m. A remaining peakedness of the density profile can be observed between 3.4 and 3.8m. The temperature profile is peaked, with a maximum of 11.5keV, in agreement with the ECE measurement of the temperature shown in figure 1. The maximum neutron rate is 0.95 $10^{16} s^{-1}$, and occurs at 5.9s, which is well before the stored energy reaches its maximum value. Clearly, the favorable conditions essential to the high neutron production rate decay without affecting the global confinement. The decay of the neutron rate seems, in this discharge, primarily related to the decay of the peaked density profile, and possibly an influx of impurities.

At 6.25s, a central MHD event occurs, as can be seen from the electron temperature signal measured near the plasma centre (there is a fast decrease, followed by a slower decrease on that signal). Similar events, but smaller in magnitude, occur at 5.8 and 6.15s, and can be seen as small decreases in the neutron rate. The event at 6.25s causes a strong influx of impurities which can be seen as a spike on the radiated power, and an increased level of this signal afterwards. The impurity was identified as carbon, using XUV spectroscopy. A fraction of the ICRH power is lost due to trips in the system, which occur due to the changing coupling conditions associated with the event. The discharge remains in H mode. At 6.8s there is the H to L transition, as witnessed by spikes on the radiated power and D_α signals, the drop in volume average density and the return of the stored kinetic energy to L mode values.

The significance of the MHD events is that in many PEP—H discharges the high neutron rate is terminated by such an event, rather than by the slow roll—over in the discharge shown here. The structure of the events, as observed on the electron temperature and the soft X—ray emission, is like that of a sawtooth: there is a fast collapse of the central temperature, there is an inversion radius, and there is a heat pulse propagating out to the edge. The rational q surface associated with the event has not yet been unambiguously determined. There are, in most cases, no precursor oscillations, and the post cursor oscillations show a mixture of modes. The rational surface could be the q=1 surface, in which case these events may be ordinary sawteeth. However, we do not expect the q=1 surface to be present in the discharge until about 8s. This expectation is based on the time of the onset of sawteeth in discharges without pellet injection, and on the central q value as determined by the equilibrium solver. Namely, in similar discharges without pellet injection the first sawtooth does not appear until after 8s, and in these discharges there are no earlier MHD events reminiscent of those in the PEP discharges. Alternatively, these events could be associated with the q=1.5 surface. According to the equilibrium solver, the q=1.5 surface enters the plasma at about 5.5s. Indeed, sawteeth with an inversion at the q=1.5 surface have been observed in TFTR [36], and MHD events at the q=1.5 surface have been observed in limiter PEP—L mode discharges in JET [24]. The question as to whether the MHD events, both in the limiter PEP—L discharges [37,38] and in the recent PEP discharges, are governed by a local (central) β limit, driven by the high pressure associated with the peaked profile, remains under discussion. In this context, it was observed that in similar discharges with pellet injection and peaked profiles, but with low ICRH power and low neutron production rates (and thus low central pressure), events at around 6s, with similar structure but smaller in magnitude than the events in the PEP mode discharges, also occur.

There are several indications that the neutron emission of this discharge (22490) is predominantly of thermonuclear origin. Calculations with the TRANSP [39] transport analysis code show that a neutron rate of about 1.5 $10^{15} s^{-1}$ is due to beam—plasma interactions, originating from the 2.5MW neutral beam injection. This is 16% of the total rate. Adding the beam—plasma and the thermonuclear fractions obtained from TRANSP, the experimental neutron rate is closely matched. These calculations are consistent with results from neutron spectroscopy, which show (by unfolding the neutron spectrum in pre—calculated thermal and beam—plasma parts) that about 80$\pm$10% of the neutron rate is of thermonuclear origin. The neutron spectrum also shows that a possible contribution from an ICRH induced high energy deuterium tail (via second harmonic ICRH absorption by deuterium ions) can be neglected, as expected in these high density plasmas. This is further confirmed by the absence of strong lines in the γ ray spectrum in the 500keV to 10MeV range. The γ spectrum further shows that there is no contribution from proton—beryllium fusion reactions in these discharges.

Values for the fusion product $n_D\ \tau_E\ T_i$ were obtained, where n_D is the deuterium density (an assumed 5% hydrogen minority is excluded from the central n_D), and the energy confinement time τ_E is taken as W / (P —dW/dt), where W is inclusive of fast particles originating from the neutral beam injection. The value of $n_D\ \tau_E\ T_i$, at 5.9s (the time of the maximum neutron rate) is between 7.0 and 8.6 10^{20} m^{-3} s keV ($n_D = 8\ 10^{19} m^{-3}$, $\tau_E = 1.03$s, T_i between 8.5 and 10.5keV, to bracket the error—bars of these measurements). A TRANSP calculation with these values, and with experimentally obtained profiles of density and temperature, leads to a close match between the calculated and the experimental neutron rate. If the fast particle fraction is subtracted from the stored energy in the calculation of τ_E, the value of $n_D\ \tau_E\ T_i$ is between 5.6 and 6.8 10^{20} m^{-3} s keV. The value of Q_{D-D} (D—D fusion power divided by loss power P — dW/dt) is 1.5 10^{-3}.

A prediction of the D—T performance of this discharge, assuming the deuterium to be replaced by a 50% / 50% mixture of deuterium and tritium, can be made on the basis of the value of $n_D\ \tau_E\ T_i$. A thermonuclear Q_{D-T} (defined as fusion power, divided by loss power) of about 0.45 would be obtained. To obtain this projection, narrow profiles for the density and temperature, as measured, are used.

L to H transitions in the PEP—H discharges are delayed with respect to the time of switching on of the auxiliary heating. The typical delay time is 500ms for discharges with auxiliary heating power of 10 to 15MW. By inserting, just after the pellet injection, a short period of higher than 15MW heating power, the delay time could, in some cases, be reduced to about 300ms. This delay time is characteristic of H modes, in particular for H modes without sawteeth. In discharges with sawteeth the transition can be triggered earlier due to the heat pulse following the sawtooth. In JET, for H modes with ICRH and without pellet injection, where the sawteeth are stabilised by the ICRH, delay times of up to 500ms have also been observed.

In figure 3 the time evolution of a discharge is shown in order to illustrate the possible consequence of this delay. Here, the pellet is fired at 5s (4mm, 3 10^{21} atoms), into a double—null X—point discharge with toroidal field 3.2T and plasma current 3.6MA. The auxiliary power is switched on at 6s, and is ramped up relatively quickly (compare with shot 22490 in figure 1). The H mode transition takes place at 6.5s (D_α trace). Already during the PEP—L phase (6 to 6.5s) a high neutron rate of 1.2 $10^{16} s^{-1}$ is obtained, at 6.45s. The neutron production rate then decreases, apparently correlated with a minor MHD relaxation taking place in the outer plasma region. The L—H transition then takes place (possibly triggered by this MHD event) and the neutron rate increases again to a maximum of 1.2 $10^{16} s^{-1}$ at 6.7s. Although in this discharge an equal neutron rate was obtained in the PEP—L and PEP—H phases, the H mode transition allowed a longer sustainment of the high neutron rate and a larger integral neutron

production. The H mode is terminated at 7s; the event at 6.7s is associated with an impurity influx. In this discharge the maximum central ion temperature is 14keV. The neutron rate does not appear to be limited by MHD phenomena, but appears to roll over with the decay of the peaked profile and possible impurity influxes. This discharge is of further interest because it shows that a good pellet enhancement is still obtained, despite the delay time of 1 second between the injection of the pellet and the switching on of the additional heating.

PEP—H modes have also been obtained with neutral beam injection. With 10.5MW of deuterium injection (8 MW at 140keV per particle and 2.5MW at 80keV), a maximum neutron production rate of $2.2\ 10^{16}$ was obtained. This corresponds to a Q_{D-D} of $2.45\ 10^{-3}$, with electron and ion temperatures about equal at 10keV.

A preliminary transport analysis of discharge 22490, at times around 6s (see figure 1) has been carried out both with the FALCON [40] and with the TRANSP transport analysis codes. The results are quoted in terms of the one—fluid thermal conductivity χ_{eff}, defined as $q_{cond} / (n_e \nabla T_e + n_i \nabla T_i)$, where q_{cond} is the heat loss flow through a flux surface and n_i is the sum of the ion densities. In the centre of the discharge χ_{eff} is of order $0.5 m^2/s$. This is considerably smaller than central χ_{eff} values obtained in standard L and H mode operation with ICRH at comparable power levels, and is similar to the values obtained in PEP limiter discharges [24,41], and in hot—ion H modes [31,32]. In the bulk of the plasma ($r/a > 0.4$) the value of χ_{eff} ($\chi_{eff} < 1.5 m^2/s$ for $r/a < 0.7$) is similar to that in standard H mode discharges and hot—ion H mode discharges [20]. This is considerably smaller than values obtained in L mode [20], including the limiter PEP—L mode discharges [24]. The transport analysis thus confirms that the good edge confinement associated with the H mode has been combined with the good central confinement that characterises the PEP mode, and the hot ion H mode.

3 OPERATIONAL ASPECTS

Several operational aspects play a role in the achievement of the PEP—H mode. First of these is the development of a discharge in which the X—point configuration is formed during or just after the plasma current rise, and clearly before the onset of sawteeth oscillations. In JET, this was a novel approach. The basic rationale is that it was observed in 1988 and 1989 experiments with PEP modes in L mode limiter discharges, that it was easier to obtain required density profiles for the PEP mode by pellet injection during or just after the current rise (ie. without sawteeth), than in the flat top of discharges, during sawtoothing. The explanation appears to be that the electron temperature profile, which is the most important factor determining the pellet ablation, is more peaked before the sawteeth than during the sawtoothing phase. As a consequence, central ablation of the pellet, which is a strict condition for obtaining a peaked density profile, is favoured in the current rise experiments. Furthermore, it has been observed on a number of occasions, that a very rapid drop of temperature can occur when the pellet enters the q=1 region [42,43]. The window for deep pellet injection in JET, with pellets of 4mm at a speed of about 1200m/s, is narrow. When the electron temperature is too high, the pellet ablates before it reaches the centre of the discharge. If the temperature is too low, the probability of incurring a radiative collapse of the plasma edge is large [44]. The correct ablation is achieved for central electron temperatures between 2.2 to 2.6keV.

In JET, the formation of an X—point magnetic configuration with sufficient triangularity to allow coupling of ICRH power, relies partly on the poloidal field created as a stray field from the central solenoid. The central section of the central solenoid is run at a higher current than the top and bottom sections, the difference current being driven by a separate power supply connected across the central coil. To avoid vertical stresses in the central solenoid, this difference current can only be used early in the discharge if the plasma start—up is performed without pre—magnetisation of the central solenoid. The plasma breakdown is generated simply by demanding maximum voltage from the solenoids power supply. This mode of operation, which is uncommon in JET, appears successful. Plasma formation was achieved at a loop voltage of about 3V (0.15V/m). The current rise was sustained with the loop voltage having a maximum value of 6V.

The ICRH antennas in JET were operated for the first time with Faraday shields made of solid Beryllium. The specific impurity influx, associated with ICRH heating [45] is reduced to negligible levels (a change of the effective ion charge Z_{eff} of about 0.005 per megawatt ICRH power [46] has been observed) with respect to the nickel screens used in previous operation.

A further operational improvement was made to facilitate the coupling of ICRH power to H modes. It has been observed, eg. in Asdex [47], that the reduction of the thickness of the scrape—off layer, at the

transition from L to H mode, results in a reduction of the coupling resistance of the ICRH antenna (this is the impedance that the antenna presents to its feeder system at the high voltage point). These transients in coupling resistance can lead to trips in the ICRH system. Previously, this problem was overcome in JET by programming a radial movement of the plasma towards the antenna at the anticipated time of the transition. Recently, a novel system was introduced in which the radial plasma position is controlled by a feedback loop which compares the measured coupling resistance with a programmable demand value. This system will automatically decrease the distance between separatrix and antenna at the L to H transition, and a constant coupling resistance is maintained. Used in conjunction with JET's automatic frequency feedback system [48], a constant complex impedance is presented to the end–stages of the RF amplifiers; the position feedback maintains a constant magnitude of the impedance and the frequency feedback maintains a constant phase, by making a small change of ICRH frequency (of order 50kHz). The positioning system also allows for fine tuning of the plasma radial position by programming the demanded coupling resistance.

4 COMPARISON WITH OTHER MODES OF OPERATION

In this section, a comparison of global energy confinement and neutron production rate, between the recently obtained PEP mode discharges and other modes of operation, is presented. We note a priori, that a clear H mode signature is not obtained in all recent PEP discharges. In some cases, the D_α signature is that of an elmy H mode, in other cases, the D_α signature is inconclusive as to the confinement mode and/or the time of an L to H transition. There is a continuum between PEP—L, elmy PEP—H and clear PEP—H mode discharges. However in the best cases (in terms of confinement) a clear identification as an H mode is possible. These difficulties with the reproducibility of the H mode, and the absence of a clear signature on the D_α signal, may have to do with the proximity of the separatrix to the ICRH antenna and the belt limiter (the absence of clear D_α signatures in those conditions was noted earlier in H modes with ICRH alone [49]).

In figure 4, the kinetic stored energy (from the diamagnetic loop), divided by the plasma current to normalise for the current dependence W_{dia}/ I_{plasma}, is shown versus the loss power $P_{tot} - dW_{dia}/dt$. The solid and dashed lines indicate the Goldston scaling [5] (substituting loss power for the total input power) for these discharges, with a multiplier of 1 (L mode) and 2 (H mode) respectively, as a guide to the eye. The confinement is shown for typical L mode (limiter data with 3MA plasma current at about 2.8T toroidal field, deuterium plasmas with ICRH heating alone, not pellet—enhanced), and typical H mode (X—point discharges at 3MA plasma current and toroidal field between 2.2 and 3.0T, deuterium plasmas with ICRH heating alone, not pellet—enhanced). Typically the 3MA limiter L mode data is somewhat enhanced over the Goldston L mode scaling. This is in part due to fast particle pressure from the ICRH minority tail, in discharges with relatively low density. The 3MA H mode data scatters around the two times Goldston line. A number of PEP—L mode discharges, obtained in limiter operation (3MA plasma current, 3.3T toroidal field, ICRH heating alone or ICRH heating plus less than 2.7MW NBI) in the 1988 experimental campaign is included. There is, on average, a slight enhancement in confinement of the 1988 PEP—L mode data with respect to the standard L mode data. All points for these data classes are shown at the time of the maximum stored energy W_{dia}; there is one point per discharge.

The recent PEP data is represented by the open triangles and, for selected discharges, by the closed symbols. The open triangles, at one point per discharge show the datapoints at maximum stored energy. The scatter in these datapoints arises for two reasons: first, there is the previously mentioned continuum of discharges between PEP—L and PEP—H mode; second, for some discharges the maximum of the stored energy occurs in the pellet—enhanced phase (where both neutron rate and global energy

confinement are enhanced) while for others, the maximum stored energy is obtained after the pellet–enhanced phase, when the peaked profile has disappeared.

To elucidate the confinement properties of the PEP discharges further, additional datapoints are shown for selected discharges. The solid stars represent the confinement at the time of the maximum of the neutron production rate. This occurs, for these discharges, clearly before the stored energy reaches its maximum (as eg., in the discharge in figure 1). These confinement points are therefore transient, meaning here that the dW/dt term is a considerable fraction (typ. >30%) of the total input power. Good confinement is observed in this early stage; the best of the transient points correspond to two to three times Goldston scaling.

For the same discharges, the points of maximum stored energy are pointed out by arrows; in these four cases, the maximum of the stored energy occurs after a clear L to H transition, and occurs after the maximum of the neutron production, but still during the pellet enhanced phase. The confinement obtained here is enhanced over the typical H mode confinement. The subsequent transition from PEP–H to normal H confinement is shown by the closed triangles, which represent the confinement after the PEP enhancement has decayed (note that for two of the four selected discharges a point can not be shown, because the H phase was terminated together with the PEP phase, by an MHD event). After the PEP phase the confinement of these discharges corresponds to ordinary H mode confinement.

We thus conclude that the best PEP–H modes, after a transient phase of strongly enhanced confinement (the stars), reach a maximum stored energy which is better than that of typical H modes (the open triangles), and reach, after the PEP enhancement decays, a confinement state equal to that of ordinary H modes.

In figure 5, the neutron production rate is shown versus the kinetic stored energy for the same categories of data. There is one datapoint per shot, taken at the time of maximum neutron rate. The NBI power for all points in this plot is less than 2.7MW (at 80keV per particle, the level required for diagnostic purposes), while all data obtained after downward transients of the NBI power is excluded. The neutron rate, associated with beam plasma reactions of the slowing down beam ions, is estimated (by calculations with the TRANSP code, see also section 2), to be less than $1.5\ 10^{15}\ s^{-1}$. Some points are with ICRH alone. There is no distinction between 3MA and 3.5MA plasma current. We see, that the neutron rate, both of the 1988 PEP–L limiter discharges and of the recent PEP discharges is enhanced by a factor up to 5 with respect to the non–enhanced discharges, even if the beam driven yield is subtracted for the recent PEP discharges. Further, a clear trend of the neutron rate with the stored energy is observed, and in fact, the trends are similar for the 1988 PEP data and the recent PEP data; higher neutron rates have been obtained in the recent experiments primarily because the stored energy was higher. For the same stored energy, the peak neutron production appears not to depend strongly on whether the discharge is in the PEP–L mode or in the PEP–H mode, although, naturally, in the H mode the stored energy is obtained for a lower value of the input power. This point is strengthened by

the observation that plots of neutron rate versus total input power or loss power show appreciably more scatter than the plot versus stored energy shown here.

The solid triangles in the plot show the neutron rate of some of the recent PEP discharges after the PEP enhancement has disappeared. These points represent the same discharges and times as the solid triangles in figure 4. We thus observe that the neutron rate of these discharges is similar to that of the typical H mode discharges.

We conclude that during the pellet—enhanced phase of the PEP—H discharges a strong enhancement of the neutron production rate, and a moderate enhancement of the global H mode energy confinement is obtained. The neutron production rate correlates well with the stored energy of the discharge. In section 2 it was argued that after decay of the PEP phase, ordinary H mode discharges are obtained. This is confirmed here by the similarity of the neutron rate and the confinement of the 'post—PEP—H' discharges to those of ordinary H mode discharges.

5 CONCLUSIONS

It has been shown in this paper that two principal regimes of enhanced tokamak performance, namely the pellet enhanced performance mode and the H confinement mode have been successfully combined. High fusion reactivity was obtained in a regime where the electron and ion temperatures are approximately equal; the high neutron production rate is predominantly of thermonuclear origin. A fusion product $n_D \tau_E T_i$ of between 7 and 8.6 10^{20} m^{-3} s keV (including fast particles in the energy confinement, and using P_{loss} in the evaluation of the energy confinement time) was obtained in a PEP—H mode with 9MW ICRH and 2.5MW NBI. This is the highest value achieved in JET for operation under the condition of equal electron and ion temperatures. The corresponding thermonuclear Q_{D-T}, assuming the discharge was to be run in a deuterium— tritium fuel mixture (50% /50%), is about 0.45. This number was evaluated assuming realistically peaked profiles. The PEP—H mode, as well as most of the PEP—L modes in JET, are achieved in sawtooth—free discharges. The maximum neutron rate of PEP discharges correlates well with the stored energy of the discharge. The indications are that similar neutron rates can be obtained for PEP—L and PEP—H modes, at the same stored energy. In the PEP—H mode, a given value of the stored energy is obtained for a lower input power than in a PEP—L mode. Furthermore, there is an indication that in the PEP—H mode the duration of the enhanced phase, and thus the integral number of neutron, is larger than in PEP—L modes. It has been shown for PEP—H modes that, after the pellet—enhancement decays, the discharge becomes an ordinary H mode discharge, with confinement and neutron rate similar to that of non—pellet—enhanced H mode discharges. It has also been shown that the PEP—H mode is obtained when the switching on of the additional heating is delayed with respect to the pellet injection. Delay times of up to 1s, corresponding to about 2 (ohmic) energy confinement times, have been used.

The pellet—enhanced performance in H mode is a transient phenomenon, as it is in L mode. The enhanced phase is terminated either by a gradual decrease of the ion temperature and neutron rate under the influence of the decay of the peaked profile and possibly impurity influxes, or by a fast decrease of temperature and neutron rate by MHD phenomena. The nature of the MHD events is not understood. There are indications that primarily a m=3, n=2 mode may be responsible for the collapse of the central plasma parameters. It is not clear whether this mode is driven by the central kinetic pressure. In any case, the H mode persists following the termination of the PEP—H phase.

Several technical and operational developments have facilitated the achievement of the PEP—H mode; first, in order to achieve X—point operation early in the discharges, ie. before the onset of the sawteeth, plasma start—up at low loop voltage, without pre—magnetisation of the central solenoid, was established; second, for the first time, the ICRH system is operated with Faraday screens made of solid beryllium, in

order to eliminate ICRH—generated impurity influxes; third, a novel system for the plasma radial position control has been developed, in which the plasma position is controlled by the ICRH coupling resistance.

Most of the proposed next step tokamaks need H mode energy confinement in order to ignite. It is therefore significant that the enhancement of fusion reactivity, obtained with the PEP mode, has been shown to be compatible with H mode operation. If the integral fusion energy from a PEP—H mode exceeds that of a PEP—L mode, as was argued above, an additional advantage over L mode operation is obtained. The PEP—H mode should be considered as a potential element of ignition strategy in future tokamak devices. This is so in particular for those tokamaks that aim to operate at moderate plasma currents and to utilise short ignited phases. Further work in this area should focus on realistically assessing, and further increasing, the scope of this element.

ACKNOWLEDGEMENTS

The authors acknowledge the support of the entire JET team, in particular of the members of the experimental and operational divisions that have contributed to these results. We are grateful to P. Noll, G. Bosia, A. Sibley and the CODAS division for implementing and commissioning the radial position control system. We thank T. Wijnands for assistance with the database analysis.

Pellet injection work in JET is performed under a collaboration agreement between JET and the United States Department of Energy.

REFERENCES

[1] TOSCHI, R., and NET team, Fusion Eng. and Des. **11** (1988) 47.

[2] PARKER, R., and CIT group, in Plasma Physics and Controlled Nuclear Fusion Research 1988 (proc. 12'th Int. Conf. Nice, 1988), Vol. 3, IAEA, Vienna (1989) 341.

[3] COPPI, B., and Ignitor program group, in Plasma Physics and Controlled Nuclear Fusion Research 1988 (proc. 12'th Int. Conf. Nice, 1988), Vol. 3, IAEA, Vienna (1989) 369.

[4] TOMABECHI, K., and ITER team, in Plasma Physics and Controlled Nuclear Fusion Research 1988 (proc. 12'th Int. Conf. Nice, 1988), Vol. 3, IAEA, Vienna (1989) 215.

[5] GOLDSTON, R., Plasma Physics and Controlled Fusion, **26** (1984) 87.

[6] KAYE, S.M., Survey of energy confinement scaling expressions, ITER specialists meeting, Garching, FRG, may 1988.

[7] POST, D.E. and ITER team, in Plasma Physics and Controlled Nuclear Fusion Research 1990 (Proc 13'th Int. Conf. Washington, 1990), paper IAEA—CN—53/F—1—3, IAEA, Vienna, to be published.

[8] REBUT, P.H. LALLIA, P.P. WATKINS, M.L., in Plasma Physics and Controlled Nuclear Fusion Research 1988 (proc. 12'th Int. Conf. Nice, 1988), Vol. 2, IAEA, Vienna (1989) 191.

[9] REBUT, P.H. LALLIA, P.P., Fusion Eng. and Design, **11** (1988) 1.

[10] WAGNER, F., BECKER, G., BEHRINGER, K., et al., Phys. Rev. LETT. **49** (1982) 1408.

[11] KAYE, S., BELL, M.G., BOL, K., et al., J. Nucl. Mater. **121**, (1984) 115.

[12] SENGOKU, S., and JFT—2M team, J. Nucl. Mater. **145—147** (1987) 556.

[13] TANGA, A., BARTLETT, D.V., BEHRINGER, et al., in Plasma Physics and Controlled Nuclear Fusion Research 1986 (Proc. 11'th Int. Conf. Kyoto, 1986), Vol. 1, IAEA, Vienna (1987) 65.

[14] BURRELL, K.H., EJIMA, S., SCHISSEL, D.P., et al., Phys. Rev. Lett. 59 (1987) 1432.

[15] KISHIMOTO, K., and JT—60 team, in Plasma Physics and Controlled Nuclear Fusion Research 1988 (proc. 12'th Int. Conf. Nice, 1988), Vol. 1, IAEA, Vienna (1989) 67.

[16] BUSH, C.E., BRETZ, N., McGUIRE, K., et al., in Plasma Physics and Controlled Nuclear Fusion Research 1990 (Proc 13'th Int. Conf. Washington, 1990), paper IAEA—CN—53/A—4—5, IAEA, Vienna, to be published.

[17] ASDEX team, Nuclear Fusion, **29** (1989) 1959.

[18] BURRELL, K.H., ALLEN, S.L., BRAMSON, G., Plasma Physics and Controlled Fusion, **31** (1989) 1649.

[19] KEILHACKER, M., and JET team, in Plasma Physics and Controlled Nuclear Fusion Research 1988 (proc. 12'th Int. Conf. Nice, 1988), Vol. 1, IAEA, Vienna (1989) 159.

[20] WATKINS, M. L., BALET, B., BHATNAGAR, V.P., et al., Plasma Physics and Controlled Fusion, **31** (1989) 1713.

[21] FURTH, H.P., Plasma Physics and Controlled Fusion, **28** (1986) 1305.

[22] REBUT, P.H. and JET team, in Plasma Physics and Controlled Nuclear Fusion Research 1986 (Proc. 11'th Int. Conf. Kyoto, 1986), Vol. 1, IAEA, Vienna (1987) 31.

[23] SCHMIDT, G.L., MILORA, S.L., ARUNASALAM, V., et al.,in Plasma Physics and Controlled Nuclear Fusion Research 1986 (Proc. 11'th Int. Conf. Kyoto, 1986), Vol. 1, IAEA, Vienna (1987) 171.

[24] SCHMIDT, G.L. and JET team, in Plasma Physics and Controlled Nuclear Fusion Research 1988 (proc. 12'th Int. Conf. Nice, 1988), Vol. 1, IAEA, Vienna (1989) 215.

[25] SENGOKU, S., NAGAMI, M., ABE, M., Nuclear Fusion, **25**, (1985) 1475.

[26] NAGAMI, M., Plasma Physics and Controlled Fusion, 31 (1989) 1597.

[27] ODAJIMA, K., FUNAHASHI, A., HOSHINO, K., et al, in Plasma Physics and Controlled Nuclear Fusion Research 1986 (Proc. 11'th Int. Conf. Kyoto, 1986), Vol. 1, IAEA, Vienna (1987) 151.

[28] TANGA, A., BALET, B., BARTLETT, D.V., in Controlled Fusion and Plasma Heating (Proc. 17'th Eur. Conf. Amsterdam, 1990), Vol. 14B, part 1, European Physical Society (1990) 259.

[29] BELL, M.G., ARUNASALAM, V., BARNES, C.W., et al., in Plasma Physics and Controlled Nuclear Fusion Research 1988 (proc. 12'th Int. Conf. Nice, 1988), Vol. 1, IAEA, Vienna (1989) 27.

[30] LOWRY, C.G., BOYD, D.A., CHALLIS, C.D., et al., in Controlled Fusion and Plasma Physics (Proc. 16'th Eur. Conf. Venice, 1989), Vol. 13B, part 1, European Physical Society (1989) 87.

[31] KEILHACKER, M., and JET team, Phys. Fluids B **2** (1990) 1291.

[32] TANGA, A., and JET team, in Plasma Physics and Controlled Nuclear Fusion Research 1990 (Proc 13'th Int. Conf. Washington, 1990), paper IAEA—CN—53/A—4—1, IAEA, Vienna, to be published.

[33] THOMAS, P., and JET team, in Plasma Physics and Controlled Nuclear Fusion Research 1990 (Proc 13'th Int. Conf. Washington, 1990), paper IAEA—CN—53/A—5—3, IAEA, Vienna, to be published.

[34] JACQUINOT, J. and JET team, Plasma Physics and Controlled Fusion, **30** (1988) 1467.

[35] SALZMANN, H., BUNDGAARD, J., GADD, A., et al., Rev. Scientific Instr. **59**, (1988) 1451.

[36] McGUIRE, K., ARUNASALAM, V., BELL, M.G., in Plasma Physics and Controlled Nuclear Fusion Research 1986 (Proc. 11'th Int. Conf. Kyoto, 1986), Vol. 1, IAEA, Vienna (1987) 421.

[37] GALVAO, R.M.O., GOEDBLOED, J.P., HUYSMANS, G., LAZZARO, E., O'ROURKE, J., SCHMIDT, G.L., SMEULDERS, P., in Controlled Fusion and Plasma Physics (Proc. 16'th Eur. Conf. Venice, 1989), Vol. 13B, part 1, European Physical Society (1989) 501.

[38] CHARLTON, L.A., BAYLOR, L.R., HOULBERG, W.A., MHD analysis of peaked pressure profiles produced by pellet injection in JET, submitted to Nuclear Fusion.

[39] HAWRYLUK, R.J., Proceedings Course and Workshop, Varenna, (1979) 19.

[40] TIBONE, F., BALET, B., CORDEY, J.G., et al., in Controlled Fusion and Plasma Physics (Proc. 16'th Eur. Conf. Venice, 1989), Vol. 13B, part 1, European Physical Society (1989) 283.

[41] HAMMET, G.W., COLESTOCK, P.L., GRANETZ, R.S.,, et al., in Controlled Fusion and Plasma Physics (Proc. 16'th Eur. Conf. Venice, 1989), Vol. 13B, part 1, European Physical Society (1989) 131

[42] SCHMIDT, G.L., BAYLOR, L.R., HAMMET, G.W., HULSE, R., OWENS, D.K., Proceedings of IAEA Technical Committee Meeting, Gut–Ising, FRG, (1988).

[43] CHEETHAM, A.D., CAMPBELL, D.J., GONDHALEKAR, A., GOTTARDI, N., GRANETZ, R.S., MORGAN, P.D., O'ROURKE, J., in Controlled Fusion and Plasma Physics (Proc. 14'th Eur. Conf. Madrid, 1987), Vol. 11D, part 1, European Physical Society (1987) 205.

[44] TUBBING, B.J.D., BAYLOR, L., EDWARDS, A., et al., Bull. Am. Phys. Soc. **33** (1988) 2030.

[45] D'IPPOLITO, D., MYRA, J., Proc. IAEA Technical Committee Meeting on Fusion Eng. and Design, Garching, FRG (1989).

[46] START, D.F.H. and JET team, in Plasma Physics and Controlled Nuclear Fusion Research 1990 (Proc 13'th Int. Conf. Washington, 1990), paper IAEA–CN–53/E–2–1–1, IAEA, Vienna, to be published.

[47] STEINMETZ, K., NOTERDAEME, J.M., WAGNER, F., Phys. Rev. Lett. **58** (1987) 124.

[48] BOSIA, G., SCHMID, M., FARTHING, J., et al., Fusion Eng. and Design **11** (1988) 459.

[49] TUBBING, B.J.D., JACQUINOT, J.J., STORK, D., TANGA, A., Nuclear Fusion **29** (1989) 1953.

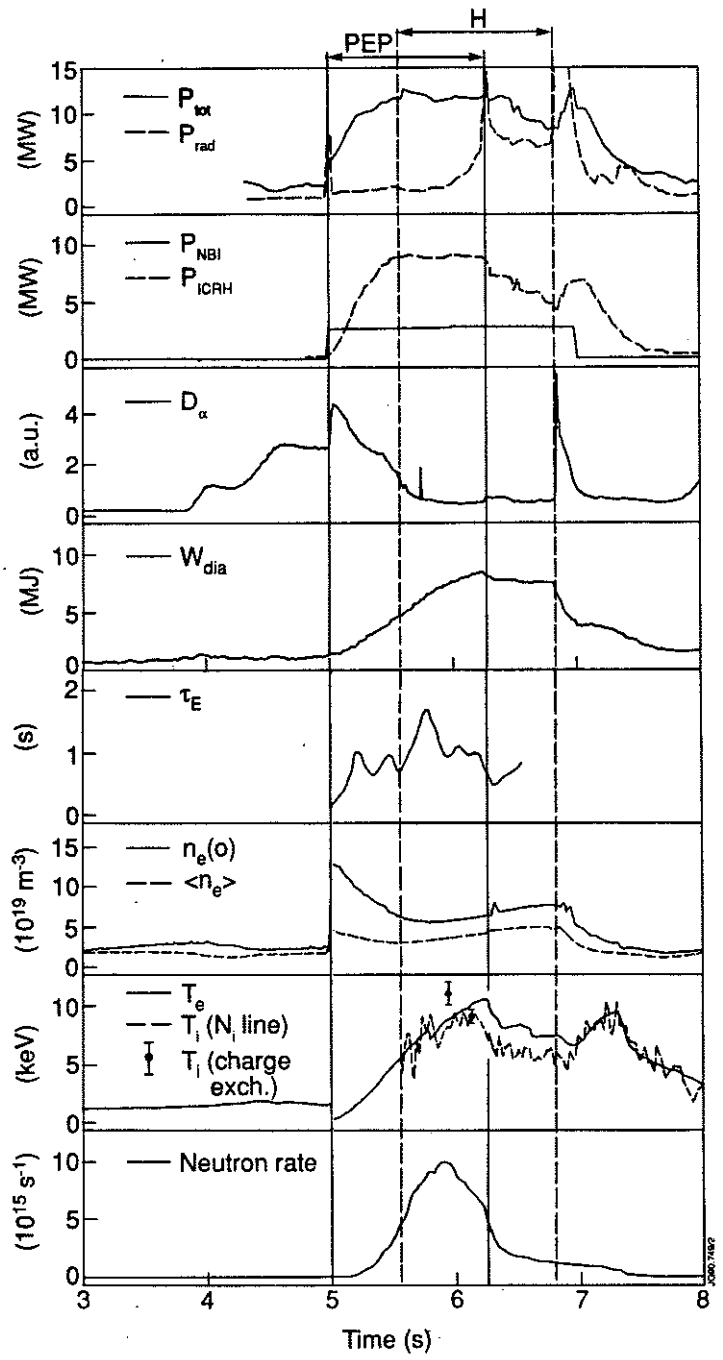

FIG. 1. Time traces of the relevant signals for the PEP–H mode discharge 22490. Shown are: the total input power and the total radiated power, the NBI power and the ICRH power, the D_α emission as measured by a vertical channel viewing near the X–point target region, the total kinetic plasma energy as measured by the diamagnetic loop, the energy confinement time defined as W_{dia} / P_{loss}, the central and volume–average electron density from a laser interferometer, the electron temperature from ECE and the ion temperature from He–like nickel radiation line–broadening and charge exchange recombination spectroscopy, the total neutron production rate measured by the neutron dosimetry. The vertical lines indicate the duration of the PEP and H phases respectively. The ECE temperature is shown for a channel that has a radial position corresponding to the temperature maximum at about 6s. The ion temperature from the nickel line is subject to an upward correction of order 1 to 2keV, due to burn–out of the He–like line. In this discharge, the toroidal field is 2.8T and the plasma current is 3MA.

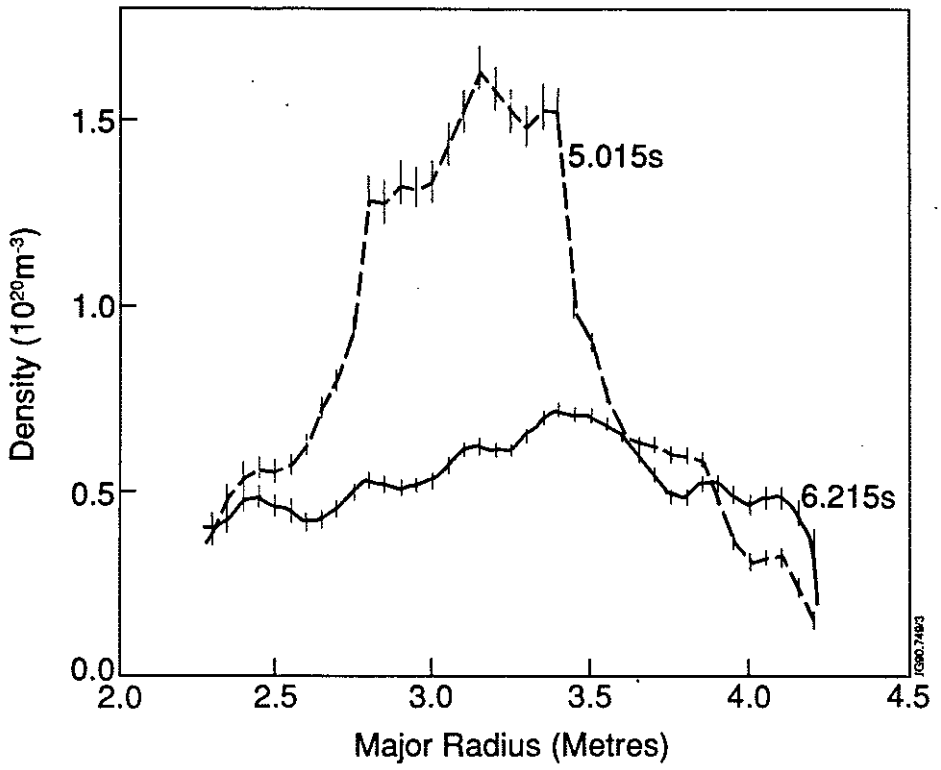

FIG. 2a. The density profiles in discharge 22490 just after pellet injection (5.0s) and at the end of the PEP—H phase (6.2s). These profiles are measured with the LIDAR time—of—flight Thomson scattering system. Error bars are shown.

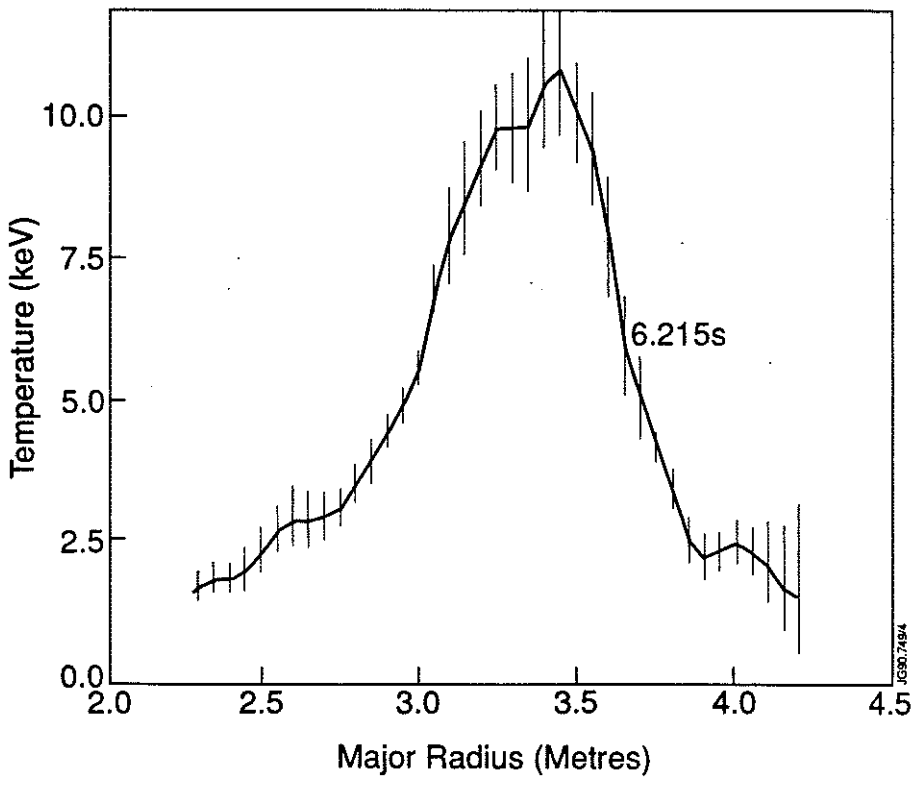

FIG. 2b. The electron temperature profile in discharge 22490 at 6.2s, measured by the LIDAR time—of—flight Thomson scattering system, at the end of the PEP—H phase. Error bars are shown.

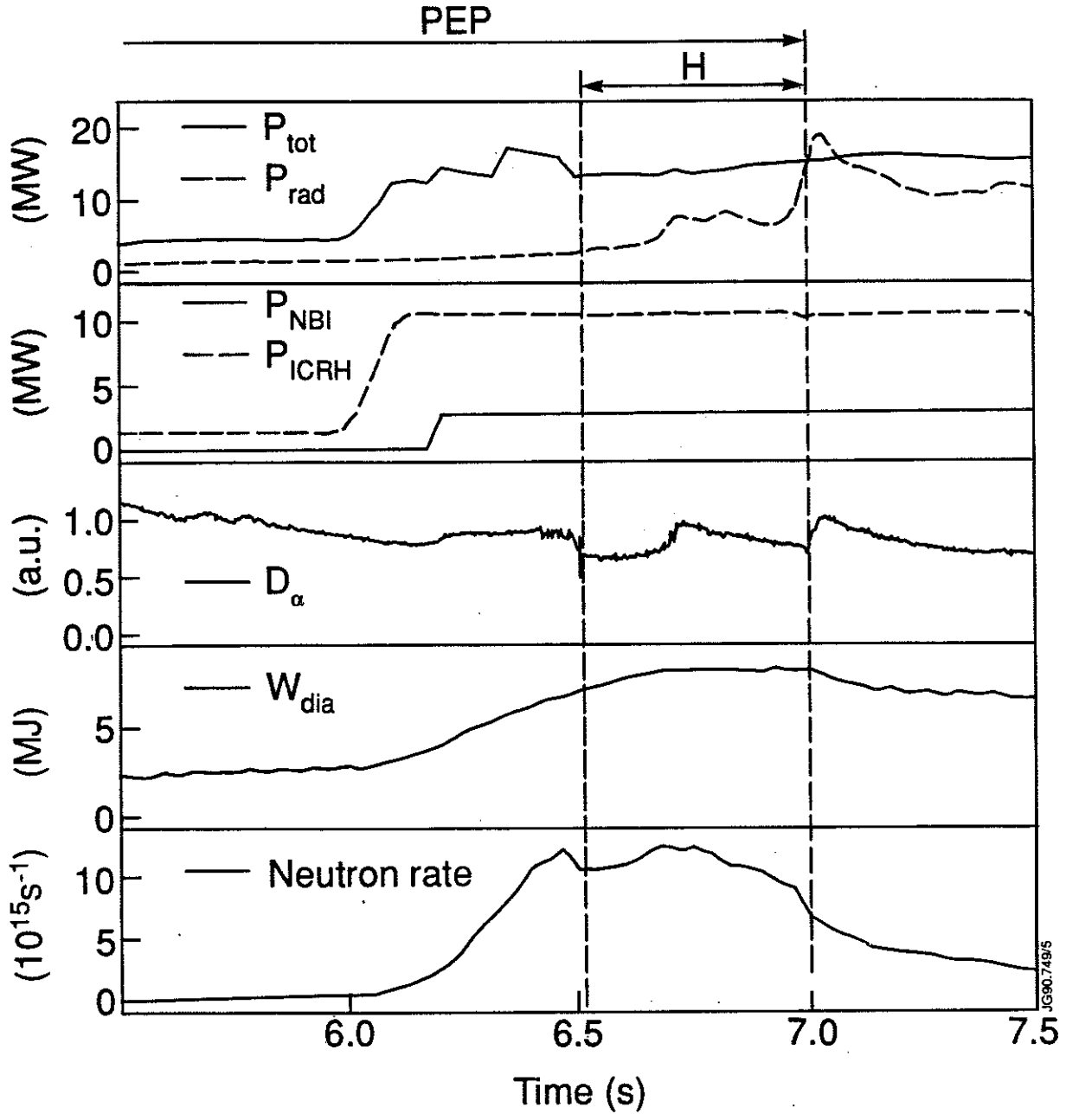

FIG. 3. Time traces of relevant signals for the PEP—H mode discharge 23098. Shown are: the total input power and the total radiated power, the NBI power and the ICRH power, the D_α emission measured by a vertical channel viewing near the X—point target area, the total kinetic plasma energy as measured by the diamagnetic loop, the total neutron production rate measured by the neutron dosimetry. The vertical lines indicate the duration of the PEP and H phases.

In this discharge, the toroidal field is 3.2T and the plasma current is 3.6MA.

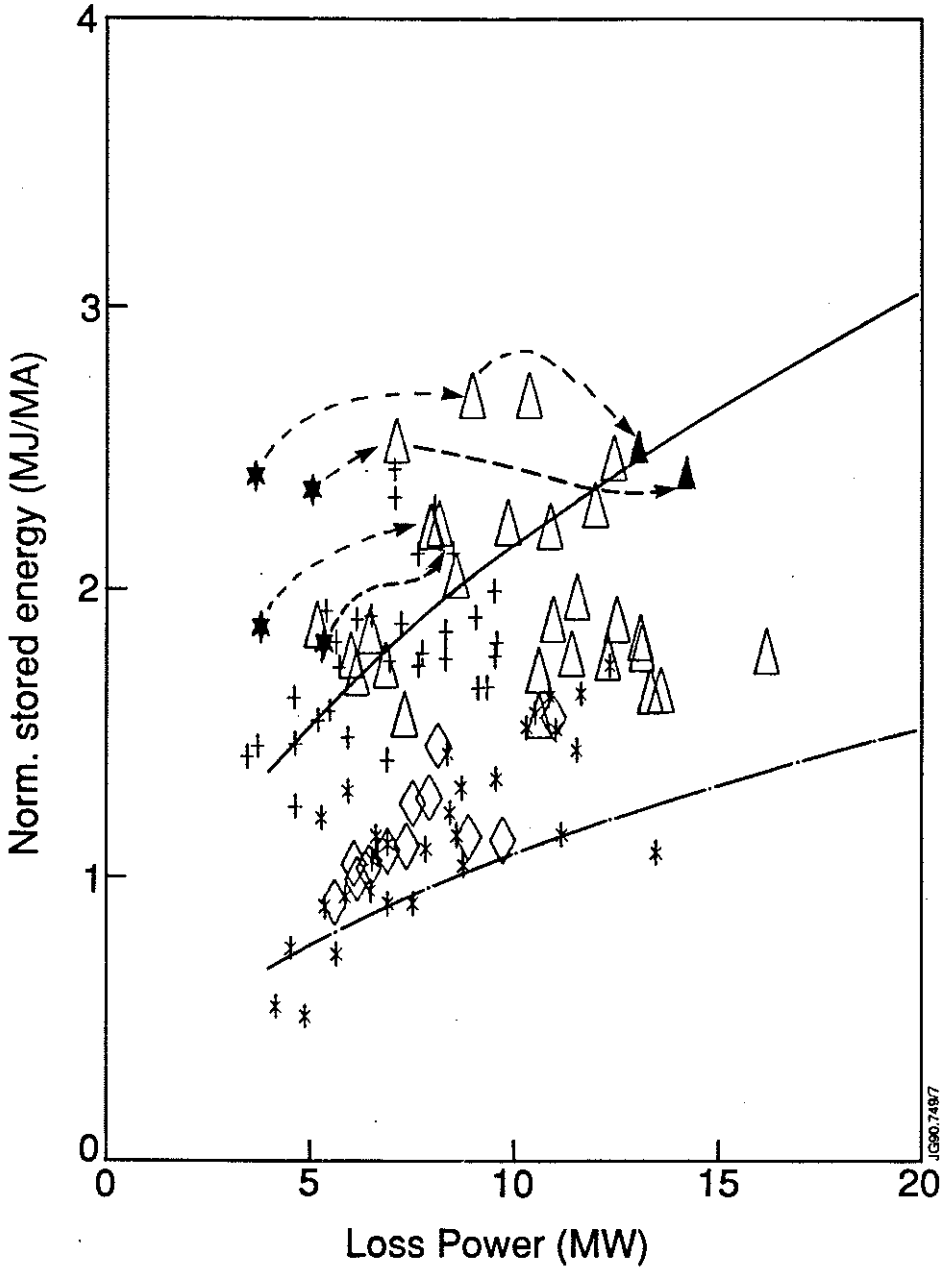

FIG. 4. A confinement overview of the recent PEP discharges. Shown is the total kinetic plasma energy (diamagnetic loop), normalised on the plasma current, versus the loss power (total input power minus time derivative of the stored energy). For comparison, sets of typical L mode and typical H mode discharges, under similar conditions and with ICRH heating alone are shown, as well as a set of PEP—L mode limiter discharges. The lines represent the Goldston confinement scaling with a multiplier of one (L mode) and two (H mode) respectively. Datapoints are one per discharge, and are taken at maximum stored energy, unless otherwise indicated. For selected discharges, additional datapoints are shown at maximum neutron rate and after the decay of the PEP mode. The arrows join the points at different timeslices of these discharges.

$*$ typical L mode, $+$ typical H mode, $\diamond$ limiter PEP—L mode.

Δ PEP mode at maximum diamagnetic stored energy.

$\bigstar$ PEP mode at maximum neutron production rate.

$\blacktriangle$ PEP mode discharges after decay of the pellet enhancement.

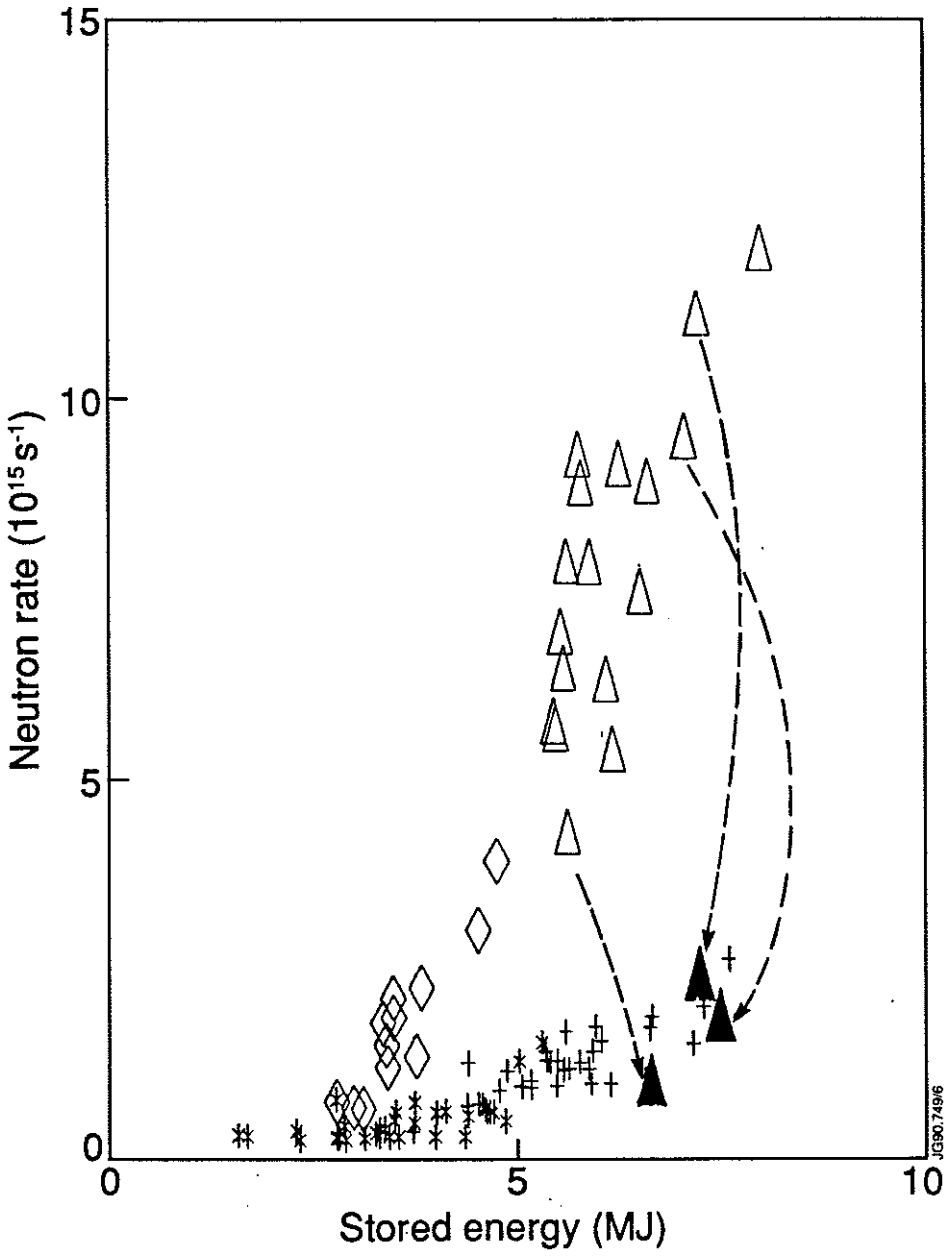

FIG. 5. The neutron production rate versus the stored energy for the recent PEP mode mode discharges with ICRH heating alone, or with ICRH plus less than 2.7MW NBI. For comparison, sets of typical L mode and typical H mode discharges with ICRH alone are shown, and a set of limiter PEP—L mode data is shown. Datapoints are one per discharge, and are taken at maximum neutron rate, unless otherwise indicated. For selected discharges, an additional datapoint is shown after the decay of the PEP mode. The arrows join the points at different timeslices of these discharges.

$*$ typical L mode, $+$ typical H mode, $\diamond$ limiter PEP—L mode.

Δ PEP mode at maximum neutron rate.

$\blacktriangle$ PEP mode discharges after decay of the pellet enhancement.

APPENDIX 1.

THE JET TEAM

JET Joint Undertaking, Abingdon, Oxon, OX14 3EA, U.K.

J.M.Adams[1], F.Alladio[4], H.Altmann, R.J.Anderson, G.Appruzzese, W.Bailey, B.Balet, D.V.Bartlett, L.R.Baylor[24], K.Behringer, A.C.Bell, P.Bertoldi, E.Bertolini, V.Bhatnagar, R.J.Bickerton, A.Boileau[3], T.Bonicelli, S.J.Booth, G.Bosia, M.Botman, D.Boyd[31], H.Brelen, H.Brinkschulte, M.Brusati, T.Budd, M.Bures, T.Businaro[4], H.Buttgereit, D.Cacaut, C.Caldwell-Nichols, D.J.Campbell, P.Card, J.Carwardine, G.Celentano, P.Chabert[27], C.D.Challis, A.Cheetham, J.Christiansen, C.Christodoulopoulos, P.Chuilon, R.Claesen, S.Clement[30], J.P.Coad, P.Colestock[6], S.Conroy[13], M.Cooke, S.Cooper, J.G.Cordey, W.Core, S.Corti, A.E.Costley, G.Cottrell, M.Cox[7], P.Cripwell[13], F.Crisanti[4], D.Cross, H.de Blank[16], J.de Haas[16], L.de Kock, E.Deksnis, G.B.Denne, G.Deschamps, G.Devillars, K.J.Dietz, J.Dobbing, S.E.Dorling, P.G.Doyle, D.F.Düchs, H.Duquenoy, A.Edwards, J.Ehrenberg[14], T.Elevant[12], W.Engelhardt, S.K.Erents[7], L.G.Eriksonn[5], M.Evrard[2], H.Falter, D.Flory, M.Forrest[7], C.Froger, K.Fullard, M.Gadeberg[11], A.Galetsas, R.Galvao[8], A.Gibson, R.D.Gill, A.Gondhalekar, C.Gordon, G.Gorini, C.Gormezano, N.A.Gottardi, C.Gowers, B.J.Green, F.S.Griph, M.Gryzinski[26], R.Haange, G.Hammett[6], W.Han[9], C.J.Hancock, P.J.Harbour, N.C.Hawkes[7], P.Haynes[7], T.Hellsten, J.L.Hemmerich, R.Hemsworth, R.F.Herzog, K.Hirsch[14], J.Hoekzema, W.A.Houlberg[24], J.How, M.Huart, A.Hubbard, T.P.Hughes[32], M.Hugon, M.Huguet, J.Jacquinot, O.N.Jarvis, T.C.Jernigan[24], E.Joffrin, E.M.Jones, L.P.D.F.Jones, T.T.C.Jones, J.Källne, A.Kaye, B.E.Keen, M.Keilhacker, G.J.Kelly, A.Khare[15], S.Knowlton, A.Konstantellos, M.Kovanen[21], P.Kupschus, P.Lallia, J.R.Last, L.Lauro-Taroni, M.Laux[33], K.Lawson[7], E.Lazzaro, M.Lennholm, X.Litaudon, P.Lomas, M.Lorentz-Gottardi[2], C.Lowry, G.Magyar, D.Maisonnier, M.Malacarne, V.Marchese, P.Massmann, L.McCarthy[28], G.McCracken[7], P.Mendonca, P.Meriguet, P.Micozzi[4], S.F.Mills, P.Millward, S.L.Milora[24], A.Moissonnier, P.L.Mondino, D.Moreau[17], P.Morgan, H.Morsi[14], G.Murphy, M.F.Nave, M.Newman, L.Nickesson, P.Nielsen, P.Noll, W.Obert, D.O'Brien, J.O'Rourke, M.G.Pacco-Düchs, M.Pain, S.Papastergiou, D.Pasini[20], M.Paume[27], N.Peacock[7], D.Pearson[13], F.Pegoraro, M.Pick, S.Pitcher[7], J.Plancoulaine, J-P.Poffé, F.Porcelli, R.Prentice, T.Raimondi, J.Ramette[17], J.M.Rax[27], C.Raymond, P-H.Rebut, J.Removille, F.Rimini, D.Robinson[7], A.Rolfe, R.T.Ross, L.Rossi, G.Rupprecht[14], R.Rushton, P.Rutter, H.C.Sack, G.Sadler, N.Salmon[13], H.Salzmann[14], A.Santagiustina, D.Schissel[25], P.H.Schild, M.Schmid, G.Schmidt[6], R.L.Shaw, A.Sibley, R.Simonini, J.Sips[16], P.Smeulders, J.Snipes, S.Sommers, L.Sonnerup, K.Sonnenberg, M.Stamp, P.Stangeby[19], D.Start, C.A.Steed, D.Stork, P.E.Stott, T.E.Stringer, D.Stubberfield, T.Sugie[18], D.Summers, H.Summers[20], J.Taboda-Duarte[22], J.Tagle[30], H.Tamnen, A.Tanga, A.Taroni, C.Tebaldi[23], A.Tesini, P.R.Thomas, E.Thompson, K.Thomsen[11], P.Trevalion, M.Tschudin, B.Tubbing, K.Uchino[29], E.Usselmann, H.van der Beken, M.von Hellermann, T.Wade, C.Walker, B.A.Wallander, M.Walravens, K.Walter, D.Ward, M.L.Watkins, J.Wesson, D.H.Wheeler, J.Wilks, U.Willen[12], D.Wilson, T.Winkel, C.Woodward, M.Wykes, I.D.Young, L.Zannelli, M.Zarnstorff[6], D.Zasche[14], J.W.Zwart.

PERMANENT ADDRESS

1. UKAEA, Harwell, Oxon. UK.
2. EUR-EB Association, LPP-ERM/KMS, B-1040 Brussels, Belgium.
3. Institute National des Récherches Scientifique, Quebec, Canada.
4. ENEA-CENTRO Di Frascati, I-00044 Frascati, Roma, Italy.
5. Chalmers University of Technology, Göteborg, Sweden.
6. Princeton Plasma Physics Laboratory, New Jersey, USA.
7. UKAEA Culham Laboratory, Abingdon, Oxon. UK.
8. Plasma Physics Laboratory, Space Research Institute, Sao José dos Campos, Brazil.
9. Institute of Mathematics, University of Oxford, UK.
10. CRPP/EPFL, 21 Avenue des Bains, CH-1007 Lausanne, Switzerland.
11. Risø National Laboratory, DK-4000 Roskilde, Denmark.
12. Swedish Energy Research Commission, S-10072 Stockholm, Sweden.
13. Imperial College of Science and Technology, University of London, UK.
14. Max Planck Institut für Plasmaphysik, D-8046 Garching bei München, FRG.
15. Institute for Plasma Research, Gandhinagar Bhat Gujat, India.
16. FOM Instituut voor Plasmafysica, 3430 Be Nieuwegein, The Netherlands.
17. Commissiariat à L'Energie Atomique, F-92260 Fontenay-aux-Roses, France.
18. JAERI, Tokai Research Establishment, Tokai-Mura, Naka-Gun, Japan.
19. Institute for Aerospace Studies, University of Toronto, Downsview, Ontario, Canada.
20. University of Strathclyde, Glasgow, G4 ONG, U.K.
21. Nuclear Engineering Laboratory, Lapeenranta University, Finland.
22. JNICT, Lisboa, Portugal.
23. Department of Mathematics, Univeristy of Bologna, Italy.
24. Oak Ridge National Laboratory, Oak Ridge, Tenn., USA.
25. G.A. Technologies, San Diego, California, USA.
26. Institute for Nuclear Studies, Swierk, Poland.
27. Commissiariat à l'Energie Atomique, Cadarache, France.
28. School of Physical Sciences, Flinders University of South Australia, South Australia SO42.
29. Kyushi University, Kasagu Fukuoka, Japan.
30. Centro de Investigaciones Energeticas Medioambientales y Techalogicas, Spain.
31. University of Maryland, College Park, Maryland, USA.
32. University of Essex, Colchester, UK.
33. Akademie de Wissenschaften, Berlin, DDR.

CR 88.49.1A